Amphiphilic Diblock Copolymers Functionalized with Strong Push−Pull Azo Chromophores: Synthesis and Multi-Morphological Aggregation

Dongrui Wang, Huifeng Ren, Xiaoqi Wang, and Xiaogong Wang*

Department of Chemical Engineering, Laboratory for Advanced Materials, Tsinghua University, Beijing 100084, P. R. China

Received July 11, 2008; Revised Manuscript Received October 26, 2008

ABSTRACT: This article reports the synthesis, characterization, and multimorphological aggregation of a series of amphiphilic diblock copolymers bearing strong push−pull azo chromophores. The diblock copolymers (PEG_x-*b*-PCN_y), which consist of poly(ethylene glycol) (PEG) and 2-(*N*-ethyl-*N*-(4-(4′-cyanophenylazo)phenyl)amino)ethyl methacrylate (PCN) blocks, were synthesized through atom transfer radical polymerization (ATRP) and postpolymerization azo-coupling reaction. PEG_x-*b*-PCN_y was prepared to have different hydrophilic/hydrophobic ratios ($x = 122$, $y = 24$, 62, 129, 224). Self-assembled aggregates were formed by the gradual addition of water to the solutions of the copolymers in THF. The formation process and morphology of the aggregates were characterized by DLS, SLS, SEM, and TEM. Results show that the block polymers start to form aggregates at the critical water content (CWC), which is related to the initial polymer concentration in THF and PCN block length. The morphology of the aggregates formed in the solutions is controlled by the PCN block length and preparation conditions. With the increase in the PCN length, the aggregates show different morphologies such as spherical micelles, rodlike aggregates, hollow nanotubes, and colloidal spheres. In the experimental range, a change in the polymer initial concentration in THF does not show an obvious effect on the aggregate morphology. The water-adding rate in the preparation process shows an important effect on the aggregate morphology. When the water-adding rate increases from 0.5 to 7.2 mL/h, the morphology of PEG_{122}-*b*-PCN_{129} aggregates changes from nanotubes to a mixture of giant vesicles and colloidal spheres. Some well-organized aggregates developed from the photoresponsive copolymers could have potential applications in photocontrollable drug delivery and other uses.

Introduction

Amphiphilic block copolymers are attracting more and more attention in recent years for their self-assembling features and interesting properties.[1−9] The copolymers composed of the hydrophobic and hydrophilic blocks can be prepared by anionic living polymerization,[2,6,10] atom transfer radical polymerization (ATRP),[11] and reversible addition−fragmentation chain transfer (RAFT).[12,13] One of the most interesting properties of amphiphilic block copolymers is their ability to form a variety of self-assembled aggregates.[7−9] Spherical micelle with a hydrophobic core and a hydrophilic corona formed in aqueous medium is a typical example of the aggregates. Depending on the relative length of the hydrophobic and hydrophilic blocks, the micellar aggregates have been referred to as starlike and crew-cut micelles.[5,14−17] By adjusting polymer structure and preparation conditions, multiple aggregate morphologies, such as spherical micelles, rodlike micelles, vesicles, and hollow nanotubes, have been observed.[5−9,18,19] In all of these cases, the factors such as the monomer unit structure, ratio of the hydrophobic block to the hydrophilic block, and molecular weight of the copolymers play important roles in determining the self-assembled structures. The formation of the multiple morphologies can be partially understood by considering the influence of the stretching entropy of the core-forming blocks, the repulsive interaction of the coronal chains, and the core−corona interfacial energy.[8,9,20] However, the aggregate morphologies still cannot be fully predicted from the block copolymer structures through theoretical calculation.[21,22] Preparing block copolymers with new chemical structures and studying their aggregation behavior not only gives some potentially useful materials but also leads to insight into the origin of the morphological complexity.

Azobenzene-containing polymers (azo polymers for short) have been intensively investigated in recent years.[23−25] Azo polymers can show interesting photoresponsive properties, such as phase transition,[26] chromophore orientation,[27] surface-relief-grating (SRG) formation,[28,29] photomechanical bending of thin films,[30−32] and photoinduced deformation of colloidal spheres.[33,34] The photoinduced variations are caused by the trans−cis photoisomerization of azobenzenes and subsequent responses of polymeric structures to the stimulus at different levels.[25] The properties of azo polymers are determined by both the isomerization behavior of azobenzenes and the polymeric architectures. Azo polymers with different structures have been prepared to develop or optimize these photoresponsive functions.[24,25]

Azobenzene-containing block copolymers can combine photoresponsive properties of azo polymers with self-assembling characteristics of block copolymers. In recent years, several types of azobenzene-containing amphiphilic block copolymers have been prepared by the use of ATRP and RAFT.[35−42] Amphiphilic diblock copolymers containing poly(ethylene glycol) (PEG) as the hydrophilic block and azobenzene-containing block as the hydrophobic block have been prepared.[35] Thin films of the block copolymers can show interesting phase-separation behavior.[35,43] The cylinder domains of the block copolymers can be aligned or manipulated by polarized light irradiation.[44,45] Diblock copolymers composed of azobenzene-containing polymethacrylate and poly(acrylic acid) blocks have been prepared.[36] The micellar aggregation of the block copolymers can show a reversible change upon alternating UV and visible light illumination. Azobenzenes bearing strong push−pull substituents have been classified as pseudostilbene-type azo

* Corresponding author: E-mail: wxg-dce@mail.tsinghua.edu.cn.

10.1021/ma801565e CCC: $40.75
Published on Web 11/12/2008

compounds.[46] Polymers containing such chromophores can show interesting properties such as SRG formation,[28,29] photoinduced colloidal deformation,[33,34] and optical nonlinearity.[47,48] However, monomers containing such structures are difficult to polymerize directly through ATRP because of the inhibition of the azo chromophores to free-radical polymerization. In a recent study, we used a postpolymerization azo-coupling scheme to synthesize an amphiphilic diblock copolymer containing strong push−pull-type azo chromophores.[49] The block copolymer was synthesized through the azo-coupling reaction of an aniline-bearing block precursor obtained from ATRP. Although different azobenzene-containing amphiphilic block copolymers have been prepared, a thorough investigation of the possible aggregate morphologies formed in solutions and their correlation with copolymer structures is still lacking in the literature.

In this work, a series of amphiphilic diblock copolymers that bear strong push−pull azo chromophores was synthesized by the ATRP and postpolymerization azo-coupling reaction. The copolymers (PEG_x-*b*-PCN_y) consist of a hydrophilic PEG block and a hydrophobic 2-(*N*-ethyl-*N*-(4-(4′-cyanophenylazo)phenyl)-amino)ethyl methacrylate (PCN) block. The series of the block copolymers were prepared to have the same hydrophilic block and different length hydrophobic blocks. As the hydrophobic block length was altered, the block copolymers showed the ability to form aggregates with different morphologies such as spherical micelles, rodlike aggregates, hollow nanotubes, and colloidal spheres. The polymer preparation, aggregate formation, and morphology variation will be presented in detail together with a discussion about the influence of the polymer structures and preparation conditions.

Experimental Section

Materials. Poly(ethylene glycol) monomethyl ether with a number-average molecular weight of about 5 000 was obtained from Fluka and was purified by azeotropic distillation with toluene before use. Copper(I) bromide (98%, Acros) was first washed with excess acetic acid, followed by ethanol and ether, and it was then dried. Anisole was distilled over calcium hydride prior to use. Tetrahydrofuran (THF) was purified by distillation with sodium and benzophenone. Deionized water (resistivity >18 MΩ·cm) was obtained from a Milli-Q water purification system. All other reagents and solvents were purchased commercially and used without further purification.

PEG_x-*b*-$PEMA_y$. The precursor copolymers, poly(ethylene glycol)-*block*-poly(2-(*N*-ethyl-*N*-phenylamino)ethyl methacrylate) (PEG_x-*b*-$PEMA_y$), were prepared through ATRP initiated by a macroinitiator (PEGBr). PEGBr was obtained through the reaction of PEG monomethyl ether with 2-bromo-2-methylpropionyl bromide. The repeat unit number of PEGBr was estimated to be 122 from the ^{1}H NMR spectrum (Figure S1, the Supporting Information). 2-(*N*-Ethyl-*N*-phenylamino)ethyl methacrylate (EMA) was synthesized according to the method described in a previous work.[49] PEG_x-*b*-$PEMA_y$ copolymers were then prepared through ATRP of EMA with different feed ratios of the monomer to PEGBr. The synthesis of PEG_{122}-*b*-$PEMA_{129}$ is given below as a typical example. PEGBr (0.275 g, 0.05 mmol) and CuBr (28.8 mg, 0.2 mmol) were added to a 25 mL Schlenk flask. The flask was degassed and back-filled with argon three times. Anisole (5 mL), EMA (1.75 g, 7.5 mmol), and 1,1,4,7,10,10-hexamethyltriethylenetetramine (HMTETA) (54.4 μL, 0.2 mmol) were added to the flask through gastight syringes. After it was degassed by three freeze−pump−thaw cycles, the flask was immersed in an oil bath at 80 °C for polymerization under argon atmosphere. After 10 h, the reaction was stopped by diluting with THF, and the mixture was passed through an alumina column to remove the catalyst. The polymer was purified twice by precipitation in hexane, collected by filtration, and dried in a vacuum oven for 24 h. M_n (GPC) = 21 900, M_w/M_n = 1.21, and M_n (NMR) = 35 600. ^{1}H NMR ($CDCl_3$ δ): 0.70−1.00 (m, 3H), 1.11 (t, 3H), 1.50−1.90 (m, 2H), 3.32 (m, 2H), 3.46 (t, 2H), 3.64 (m, PEG H), 4.00 (t, 2H), 6.68 (m, 3H), 7.17 (t, 2H). IR (KBr) (cm^{-1}): 2970 2890 (C−H), 1730 (C═O), 1600 1510 (benzene ring), 1130 (C−O−C).

Table 1. Molecular Weights and Distributions of the Macroinitiator and Precursor Block Copolymers

sample	M_n (GPC)	M_w/M_n (GPC)	M_n (NMR)
PEGBr	7600	1.05	5500
PEG_{122}-*b*-$PEMA_{24}$	12 900	1.15	11 100
PEG_{122}-*b*-$PEMA_{62}$	16 600	1.19	19 900
PEG_{122}-*b*-$PEMA_{129}$	21 900	1.21	35 600
PEG_{122}-*b*-$PEMA_{224}$	35 500	1.29	57 700

Table 2. Molecular Weights and Distributions of the Diblock Azo Copolymers

sample	M_n (GPC)	M_w/M_n (GPC)	M_n (NMR)	PEG/PCN (wt/wt, NMR)
PEG_{122}-*b*-PCN_{24}	15 100	1.24	14 200	39/61
PEG_{122}-*b*-PCN_{62}	23 600	1.28	27 900	20/80
PEG_{122}-*b*-PCN_{129}	26 500	1.26	52 200	11/89
PEG_{122}-*b*-PCN_{224}	39 100	1.29	86 600	6/94

Other PEG_x-*b*-$PEMA_y$ copolymers in the series were prepared under the same condition. The amounts of EMA used in the polymerizations were: 0.30 g (1.25 mmol) for PEG_{122}-*b*-PCN_{24}, 0.87 g (3.75 mmol) for PEG_{122}-*b*-PCN_{62}, and 2.91 g (12.5 mmol) for PEG-*b*-PCN_{224}. Analytical results of these three precursor copolymers are given in the Supporting Information and Table 1.

PEG_x-*b*-PCN_y. Poly(ethylene glycol)-*block*-poly(2-(*N*-ethyl-*N*-(4-(4′-cyanophenylazo)phenyl)-amino)ethyl methacrylate) copolymers (PEG_x-*b*-PCN_y) were prepared through an azo-coupling reaction between PEG_x-*b*-$PEMA_y$ and the diazonium salt of 4-aminobenzonitrile. Diblock copolymers with a well-defined structure were obtained by the addition of an excess amount of the diazonium salt, where the conversion of the anilino groups to azo chromophores could nearly reach 100%. The synthesis of PEG_{122}-*b*-PCN_{129} is given here as a typical example. An aqueous solution of sodium nitrite (0.06 g, 0.87 mmol) was added dropwise to a solution of 4-aminobenzonitrile (0.089 g, 0.75 mmol) in a homogeneous mixture of sulfuric acid (0.15 mL) and glacial acetic acid (2.25 mL). The mixture was stirred at 0 °C for 5 min. Then, the diazonium salt solution was added dropwise to a solution of PEG_{122}-*b*-$PEMA_{129}$ (0.138 g, 0.5 mmol in terms of the anilino groups) in DMF (30 mL) at 0 °C. After the reaction was carried out at the temperature for 12 h, the solution was poured in an excessive amount of 20% sodium chloride brine. The precipitate was collected and washed with water repeatedly. After it was dried, the product was dissolved in THF and then precipitated in hexane. The precipitate was collected by filtration and was then dried in a vacuum oven for 24 h. Other PEG_x-*b*-PCN_y samples in the series were prepared under similar conditions. The amounts of precursor copolymers were 0.231 g for PEG_{122}-*b*-$PEMA_{24}$, 0.160 g for PEG_{122}-*b*-$PEMA_{62}$, and 0.129 g for PEG_{122}-*b*-$PEMA_{224}$ (0.5 mmol in terms of the anilino groups) used in the azo-coupling reactions. PEG_{122}-*b*-PCN_{24} could not be directly precipitated by pouring the DMF solution in water because of the high weight fraction of the hydrophilic PEG block. In this case, the DMF solution was dialyzed against water, and the copolymer was then collected by the evaporation of water. After that, PEG_{122}-*b*-PCN_{24} was purified by dissolution in THF and precipitation with hexane several times. The molecular weights and distributions of the diblock copolymers are summarized in Table 2. Other analytical results are given as follows: PEG_{122}-*b*-PCN_{24}: ^{1}H NMR ($CDCl_3$ δ): 0.70−1.00 (m, 3H), 1.07 (t, 3H), 1.50−1.80 (m, 2H), 3.00−3.50 (m, 4H), 3.64 (m, PEG H), 4.01 (t, 2H), 6.70 (d, 2H), 7.59 (d, 2H), 7.72 (m, 4H). IR (KBr) (cm^{-1}): 2970 2890 (C−H), 2220 (C≡N), 1730 (C═O), 1600 1510 (benzene ring), 1130 (C−O−C). UV−vis (THF): λ_{max} = 443 nm. Anal. Calcd: C, 63.8; H, 7.2; N, 9.5. Found: C, 62.6; H, 7.4; N, 9.7. PEG_{122}-*b*-PCN_{62}: ^{1}H NMR ($CDCl_3$ δ): 0.70−1.00 (m, 3H), 1.07 (t, 3H), 1.60−1.90 (m, 2H), 3.10−3.50 (m, 4H), 3.64 (m, PEG H), 4.01 (t, 2H), 6.70 (d, 2H), 7.59 (d, 2H), 7.72 (m, 4H). IR (KBr)

(cm^{-1}): 2970 2890 (C−H), 2220 (C≡N), 1730 (C═O), 1600 1510 (benzene ring), 1130 (C−O−C). UV−vis (THF): λ_{max} = 443 nm. Anal. Calcd: C, 66.7; H, 6.7; N, 12.4. Found: C, 64.5; H, 6.5; N, 11.5. PEG_{122}-*b*-PCN_{129}: ^1H NMR ($CDCl_3$ δ): 0.70−1.00 (m, 3H), 1.07 (t, 3H), 1.60−1.90 (m, 2H), 3.15−3.50 (m, 4H), 3.64 (m, PEG H), 4.02 (t, 2H), 6.70 (d, 2H), 7.59 (d, 2H), 7.72 (m, 4H). IR (KBr) (cm^{-1}): 2970 2890 (C−H), 2220 (C≡N), 1730 (C═O), 1600 1510 (benzene ring), 1130 (C−O−C). UV−vis (THF): λ_{max} = 443 nm. Anal. Calcd: C, 68.0; H, 6.4; N, 13.8. Found: C, 67.0; H, 6.4; N, 13.4. PEG_{122}-*b*-PCN_{224}: ^1H NMR ($CDCl_3$ δ): 0.70−1.00 (m, 3H), 1.07 (t, 3H), 1.50−1.80 (m, 2H), 3.00−3.50 (m, 4H), 3.64 (m, PEG H), 4.00 (t, 2H), 6.70 (d, 2H), 7.59 (d, 2H), 7.72 (m, 4H). IR (KBr) (cm^{-1}): 2970 2890 (C−H), 2220 (C≡N), 1730 (C═O), 1600 1510 (benzene ring), 1130 (C−O−C). UV−vis (THF): λ_{max} = 443 nm. Anal. Calcd: C, 68.7; H, 6.3; N, 14.5. Found: C, 67.5; H, 6.2; N, 14.0.

Aggregate Preparation. PEG_x-*b*-PCN_y samples were dissolved in anhydrous THF to obtain stock solutions with concentrations of 1 g/L. A series of solutions with different concentrations were then obtained by diluting the stock solutions. To prepare the micellar aggregates, deionized water (1 mL) was gradually added to the THF solutions of PEG_x-*b*-PCN_y (1 mL) at room temperature. The water addition was performed using a syringe pump to adjust the water-adding rate. The polymer solutions were gently stirred during the water addition. Except for the cases specifically mentioned, the water-adding rate was adjusted to be 0.5 mL/h. During the processes, the light intensity scattered at 90° was recorded to probe the variation occurring in the solutions or suspensions. When the water addition was completed, excess deionized water (9 mL) was added to the suspensions to quench the structures formed. The suspensions were stocked at room temperature in air ambience for 48 h to allow the THF to evaporate slowly.

Characterization. ^1H NMR spectra were recorded on a JEOL JNM-ECA300 spectrometer (300 MHz for proton) by using $CDCl_3$ as the solvent. We determined the molecular weight of PEGBr by calculating the integration ratio between the resonance signals of methylenes (δ = 3.64) and the terminal methyl (δ = 3.36) (Figure S1 in the Supporting Information). On the basis of the molar mass of PEGBr, the molecular weight of PEG_x-*b*-$PEMA_y$ was estimated by measuring the integration ratios between the resonance signals of the anilino moieties in the PEMA block (δ = 6.68) and the signals of PEG (δ = 3.64) (Figure S2 in the Supporting Information). Because PEG_x-*b*-PCN_y and PEG_x-*b*-$PEMA_y$ had the same number of repeat units, the molecular weight of PEG_x-*b*-PCN_y was estimated from the degree of polymerization and the molecular weights of the structure units. The molecular weights and molecular weight distributions were also measured by the use of gel permeation chromatography (GPC). The GPC instrument was equipped with a refractive index (RI) detector (Wyatt Optilab rEX) and fitted with a PLgel 5 μm mixed-D column, which was calibrated by using polystyrene standards. THF was used as the eluent, and the measurements were carried out at 35 °C with an eluent flow rate of 1.0 mL/min. Fourier transform infrared (FT-IR) measurements were carried out on a Nicolet 560-IR spectrophotometer by incorporating the samples in the KBr tablets. UV−vis spectra were recorded by using an Agilent 8453 UV−vis spectrophotometer. Thermal properties of the polymers were tested by using TA Instrument DSC 2920 with a heating rate of 10 °C/min under a nitrogen atmosphere. Laser light scattering (LLS) experiments were performed on a commercial LS instrument (ALV/DLS/SLS-5022F) equipped with a multi-τ digital time correlator (ALV/LSE-5003) and a solid-state laser (Uniphase, output power = 22 mW, λ = 632.8 nm). The aggregates were investigated by dynamic light scattering (DLS) and transmission electron microscopy (TEM). For the DLS measurement, the suspensions were diluted with deionized water to proper concentrations. The TEM observation was performed on a JEOL JSM-1200EX microscope with an accelerating voltage of 120 kV. To prepare the TEM samples, a droplet of the aggregate suspensions was set on a copper grid, dried under air atmosphere, and then dried under vacuum. Only the aggregates of PEG_{122}-*b*-PCN_{24} needed to be stained with phosphotungstic acid to obtain a vivid contrast. The aggregate morphologies were also investigated by scanning electron microscopy (SEM) performed on a Hitachi S4500 electron microscope, which was operated at an accelerating voltage of 5 kV. The samples were cast on silica slides and coated with a thin layer of gold before the observation.

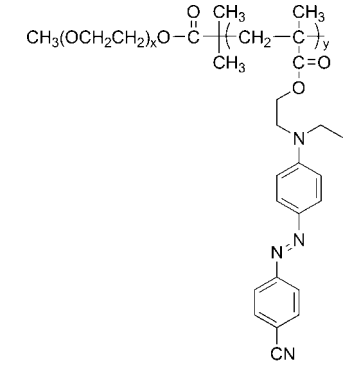

Figure 1. Chemical structure of the azobenzene-containing diblock copolymers.

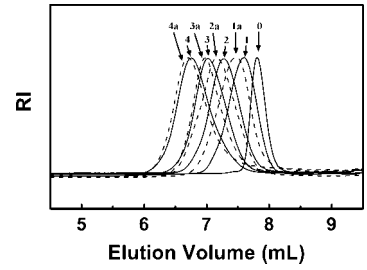

Figure 2. GPC traces of the synthesized polymers: (0) PEGBr, (1) PEG_{122}-*b*-$PEMA_{24}$, (2) PEG_{122}-*b*-$PEMA_{62}$, (3) PEG_{122}-*b*-$PEMA_{129}$, (4) PEG_{122}-*b*-$PEMA_{224}$, (1a) PEG_{122}-*b*-PCN_{24}, (2a) PEG_{122}-*b*-PCN_{62}, (3a) PEG_{122}-*b*-PCN_{129}, (4a) PEG_{122}-*b*-PCN_{224}.

Results and Discussion

Figure 1 shows the chemical structure of PEG_x-*b*-PCN_y, which consists of two covalent-linked blocks of PEG and PCN. A series of the copolymers with different compositions (x = 122 and y = 24, 62, 129, 224) was synthesized in this study. The copolymers were obtained first through ATRP initiated by a macroinitiator (PEGBr) to yield PEG_x-*b*-$PEMA_y$. Then, the precursor polymers were reacted with diazonium salt of 4-aminobenzonitrile to produce the target block copolymers. Through this synthetic strategy, block azo copolymers with well-defined structure and narrow molecular weight distribution were obtained. The characterization and aggregation behavior of the block copolymers in solution will be discussed in the following sections.

Block Copolymer Characterization. Figure 2 gives the GPC traces of PEG_x-*b*-PCN_y and other intermediate products. The GPC results show that ATRP initiated by PEGBr proceeds in a well-controlled way. After the polymerization, the peaks corresponding to PEG_x-*b*-$PEMA_y$ can be seen in the higher molecular weight ranges, and the original peak of PEGBr has completely disappeared. The molecular weight distributions of PEG_x-*b*-$PEMA_y$ become slightly broader in comparison with that of PEGBr, which is more obvious for those with the higher polymerization degree of the PEMA blocks. This reliance of the molecular weight distribution on the polymerization degree is typical for most ATRP processes.[11] After the azo-coupling reactions, the GPC peaks of PEG_x-*b*-PCN_y appear in the even higher-molecular-weight regions relative to the corresponding precursors. It implies that the azobenzene moieties are successfully introduced to the polymers. The molecular weight distributions do not show an obvious increase after the azo-coupling reactions.

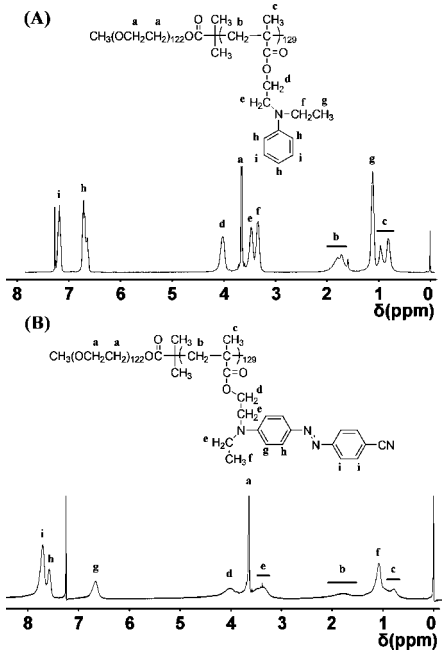

Figure 3. ^{1}H NMR spectra of (A) PEG_{122}-*b*-$PEMA_{129}$ and (B) PEG_{122}-*b*-PCN_{129} in $CDCl_3$.

The structure of PEG_x-*b*-PCN_y was determined by the spectroscopic analyses. Figure 3 shows the ^{1}H NMR spectra of PEG_{122}-*b*-$PEMA_{129}$ and PEG_{122}-*b*-PCN_{129} in chloroform as a typical example. The resonance signals corresponding to the protons on the azobenzene moieties appear in the low magnetic field region. The resonance signals of alkyl and alkene groups come out in the high magnetic field region. The assignment of the resonance signals to the protons is indicated in the Figure. The high conversion of the azo-coupling reaction is concluded by a comparison of the characteristic signals of the ^{1}H NMR spectra. The resonances of anilino protons of PEG_{122}-*b*-$PEMA_{129}$ appear at 6.68 (ortho, para) and 7.17 (meta) ppm. After the azo-coupling reaction, there are three resonances appearing at 6.70, 7.59, 7.72 ppm with the integrated intensity ratio of 1:1:2. The resonance signals of the newly introduced phenylene protons come out at the lowest magnetic field (7.72 ppm). The original signal of the protons at meta positions of the amino groups shifts to 7.59 ppm because of the increase in the conjugated length and presence of the electron-withdrawing groups. From the ^{1}H NMR spectral analysis, the conversion of the azo-coupling reaction is estimated to approach 100%. The spectra of the other PEG_x-*b*-PCN_y (Figure S3 in the Supporting Information) also show the complete conversion to form the 4-amino-4′-cyanoazobenzene moieties after the azo-coupling reactions. The results were also verified by the elemental analyses, as given in the Experimental Section.

Actual molecular weights of block copolymers can be obtained by ^{1}H NMR spectroscopy.[35] The molecular weight of PEGBr was determined from the integration ratio between the resonances of methylenes ($\delta = 3.64$) and the terminal methyl ($\delta = 3.36$). On the basis of the molar mass of PEGBr, the molecular weight of PEG_x-*b*-$PEMA_y$ was estimated from the integration ratios between the resonance signals of the anilino moieties in the PEMA block ($\delta = 6.68$) and methylene groups of the PEG block ($\delta = 3.64$). Because PEG_x-*b*-PCN_y and PEG_x-*b*-$PEMA_y$ had the same number of the repeat units, the molecular weight of PEG_x-*b*-PCN_y was obtained from the polymerization degree and the molecular weights of the repeat units. The results reveal that the block copolymers can be denoted as PEG_x-*b*-PCN_y, where $x = 122$ and $y = 24$, 62, 129, and 224. The molecular weights and distributions of the precursor copolymers and azo copolymers are summarized in Tables 1 and 2.

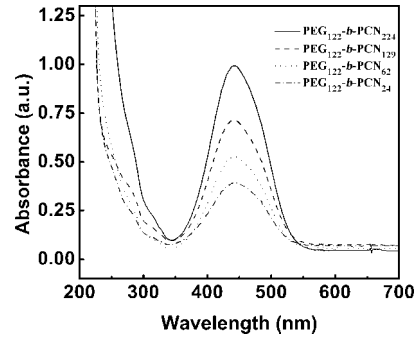

Figure 4. UV−vis spectra of PEG_x-*b*-PCN_y in THF solutions (0.01 g/L).

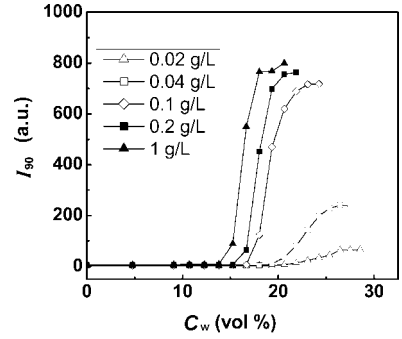

Figure 5. Plot of scattered light intensity of PEG_{122}-*b*-PCN_{129} in H_2O/THF solutions versus the water content (C_w). Each curve corresponds to a different initial polymer concentration in THF.

Figure 4 gives the UV−vis spectra of PEG_x-*b*-PCN_y in THF. All copolymers show typical spectral characteristics of the pseudostilbene-type azo chromophores. Only one strong absorption band appears in the visible wavelength range ($\lambda_{max} = 443$ nm), which can be assigned to the overlapped $\pi-\pi^*$ and $n-\pi^*$ electron transitions.[46] Because all solutions have the same concentration, the absorbance at λ_{max} reasonably increases as the PCN block length increases. The thermal analysis results are given in the Supporting Information (Figure S4). The thermal properties and their correlation with copolymer structure are discussed there.

Formation of Aggregates. We prepared the aggregates by gradually adding water to homogeneous solutions of the copolymers in THF. The method has been developed by Eisenberg et al. to prepare crew-cut micelles from amphiphilic block copolymers.[5,6] Because THF was a common solvent for both blocks of PEG_x-*b*-PCN_y, the block copolymers could be well dissolved in THF without obvious aggregation. Water was a good solvent for the PEG block but was a precipitant for the PCN block. As water was added to the PEG_x-*b*-PCN_y solutions, the solvent became progressively worse for the PCN block. When the water content reached a critical value, the copolymer solutions underwent microphase separation, and the PCN chains started to aggregate, which was reflected by a sudden increase in the scattered light intensity. To obtain well-developed aggregates, more water was continually added to the solutions to ensure that the aggregation process could be completed. After that, a large amount of water was added to the suspensions to quench the self-assembled structures. THF in the suspensions was removed by the method reported in the literature.[50]

Static light scattering was used to monitor the aggregation process of the block copolymers in solution. Figure 5 shows the experimental curves of light scattering intensity (I_{90}) variation for PEG_{122}-*b*-PCN_{129} as a function of the water content (C_w) in the solutions. All curves with different initial polymer concentrations can be identified to have three regions. When

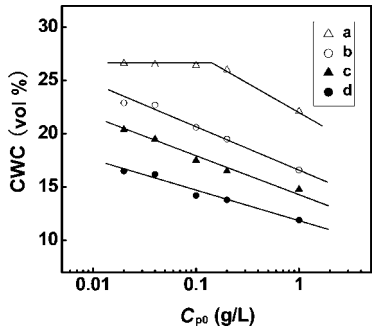

Figure 6. Plot of the critical water content (CWC) versus initial polymer concentration (C_{p0}): (a) PEG_{122}-*b*-PCN_{24}, (b) PEG_{122}-*b*-PCN_{62}, (c) PEG_{122}-*b*-PCN_{129}, (d) PEG_{122}-*b*-PCN_{224}.

the water content is relatively low, the scattered light intensity is maintained at a very low level and shows little variation, which indicates that almost no aggregation occurs in the solutions. When the water content reaches the critical value, the scattered light intensity abruptly increases because of the aggregation of polymer chains. As the water content further increases, the scattered light intensity levels off at a certain point after the rapid increase. The water content at which polymer chains start to aggregate has been defined as the critical water content (CWC).[16] From the Figure, it can be seen that the CWC is related to the initial polymer concentration (C_{p0}); that is, CWC increases as the concentration decreases. The CWC of PEG_{122}-*b*-PCN_{129} increases from 14.8 to 20.4 vol % when C_{p0} decreases from 1 to 0.02 g/L. Meanwhile, for the solutions with the higher C_{p0}, the scattered light intensity increase more rapidly as C_w increases, and the aggregation is completed by the addition of an obviously smaller amount of water.

A similar tendency of the scattered light intensity variation with the water content (C_w) was observed for the other three PEG_x-*b*-PCN_y samples. The exact relationship between CWC and C_{p0} is related to the length of the PCN blocks. Figure 6 gives a plot of the CWC as a function of C_{p0} for the block copolymers. Except for PEG_{122}-*b*-PCN_{24}, there is a linear decrease in CWC upon the increase in the logarithm of C_{p0}. A similar relationship has been reported for the aggregation of other block copolymers such as polystyrene-*b*-poly(acrylic acid).[16] For PEG_{122}-*b*-PCN_{24}, the CWC almost keeps the same value (26.5 vol %) when C_{p0} increases in a range below 0.1 g/L. When C_{p0} is greater than 0.1 g/L, the CWC starts to decrease as C_{p0} further increases. Among the four block copolymers, PEG_{122}-*b*-PCN_{24} has the shortest PCN block and highest CWC. In the range of the low C_{p0}, the initial aggregation could be dominated by the intramolecular association instead of the intermolecular combination, where the CWC does not show an obvious dependence on C_{p0}.

Morphologies of Aggregates. Morphologies of block copolymer aggregates depend on both block copolymer composition and preparation conditions, such as the copolymer concentration, type of added ions, and nature of the solvents.[5,51−53] Both factors were investigated for morphologies of PEG_x-*b*-PCN_y aggregates in this work. The effect of the PCN block length on the morphologies is discussed in this section, and the influence of the preparation conditions will be presented in the following section.

Figure 7A gives a typical TEM image of the aggregates formed from PEG_{122}-*b*-PCN_{24} with C_{p0} of 0.2 g/L. The image shows that PEG_{122}-*b*-PCN_{24} chains form spherical micelles with a size of ~20 nm. Meanwhile, some higher level aggregates formed from these small micelles can also be perceived in the picture. A statistical analysis obtained from 100 particles reveals that the number-average radius $<R>_n$ and z-average radius

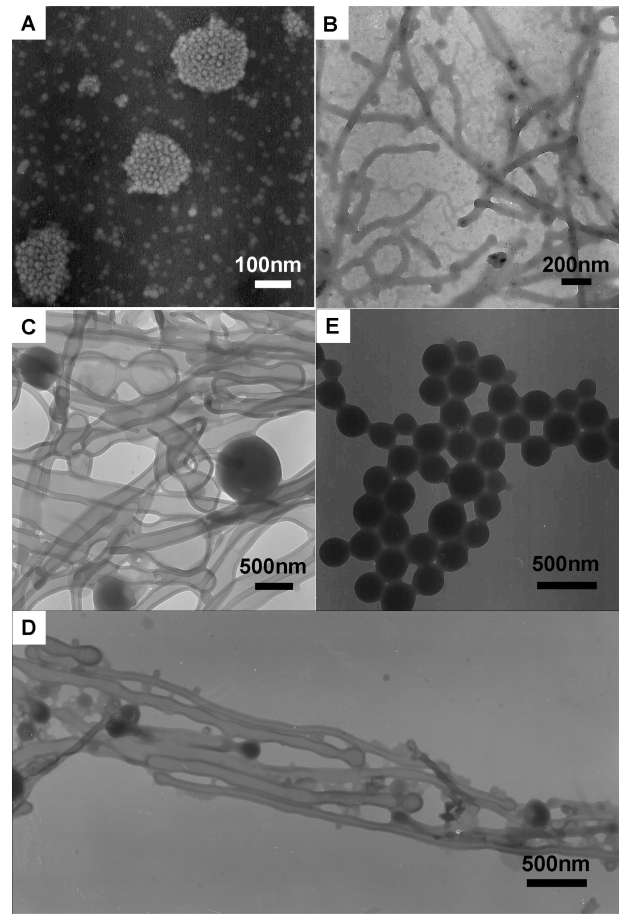

Figure 7. TEM micrographs of the aggregates: (A) PEG_{122}-*b*-PCN_{24}, C_{p0} = 0.2 g/L; (B) PEG_{122}-*b*-PCN_{62}, C_{p0} = 0.1 g/L; (C, D) PEG_{122}-*b*-PCN_{129}, C_{p0} = 0.5 g/L; (E): PEG_{122}-*b*-PCN_{224}, C_{p0} = 0.1 g/L.

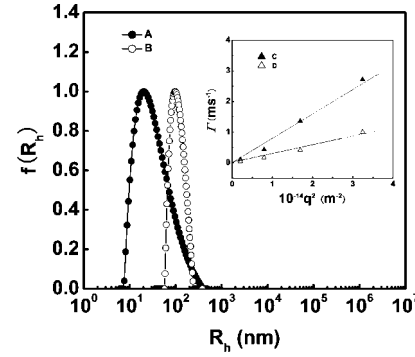

Figure 8. Hydrodynamic radius distribution of two suspensions measured at the scattering angle of 90°. (A) PEG_{122}-*b*-PCN_{24}, C_{p0} = 0.2 g/L; (B) PEG_{122}-*b*-PCN_{224}, C_{p0} = 0.1 g/L. Inset: the dependence of the average line width Γ on q^2 for the suspensions. (C) PEG_{122}-*b*-PCN_{24}, C_{p0} = 0.2 g/L; (D) PEG_{122}-*b*-PCN_{224}, C_{p0} = 0.1 g/L.

$<R>_z$ of the micelles are 9.7 and 9.8 nm, respectively. The micelles with the narrow size distribution are believed to be composed of a core of PCN blocks and a corona of the PEG blocks. Considering the relative lengths of PEG to PCN, these aggregates could be considered to be more like starlike micelles. The DLS result of the micellar suspension is shown in Figure 8 (curve A). The plot of decay rate versus squared scattering vector (inset in Figure 8, curve C) does not show any strong angular dependence, and the linear fit of the data passes through the origin. It indicates that the micelles are diffusive spherical particles in the suspension. The z-average hydrodynamic radius of aggregates $<R_h>_z$ is obtained to be 25.0 nm. In addition, the plot of hydrodynamic radius distribution measured at the

scattering angle of 90° reveals that the size distribution of aggregates is fairly board. The obviously larger aggregate size obtained from DLS could be partially attributed to the swollen PEG shells. It is also possible that the larger $<R_h>_z$ is caused by some agglomeration of the micelles in the suspension. Because the PEG corona is in absence of strong electrostatic repulsion, the micelles can agglomerate in the suspension to form clusters of micelles.

As the repeat unit number of PCN block increases, more complicated morphologies are developed from this series of block copolymers. PEG_{122}-*b*-PCN_{62} forms rodlike aggregates, and the aggregates can further organize to form some arboreal structures (Figure 7B). Some of the structures are similar to the Y junctions and cylindrical loops observed for micellar aggregates of poly(1,2-butadiene-*b*-ethylene oxide) (PB-PEO).[9] The average diameter of the rodlike aggregates is ~60 nm. PEG_{122}-*b*-PCN_{129}, which contains a significantly longer PCN block, forms hollow nanotubes with a wall thickness of about 60 nm (Figure 7C). In the Figure, the existence of the hollow space can be clearly perceived from the density contrast between the walls and inner parts. As indicated in Figure 7D, some more complicated organization also exists for the aggregates. The lengths of the hollow nanotubes are polydispersed, and some of the longest ones reach several tens of micrometers. The wall thickness is rather uniform for the hollow structures, which is ~60 nm. These morphologies are also confirmed by SEM observation (Figure S5 in the Supporting Information). Nanotubes formed in solution via self-assembly are well known for low-molecular-weight lipids and block copolymers.[21,22] However, to our knowledge, this is the first time observing that the hollow nanotubes can be formed from azobenzene-containing block copolymers.

Figure 7E gives a typical TEM image of the aggregates formed from PEG_{122}-*b*-PCN_{224} that has the longest PCN block in the series. Colloidal spheres with an average size of $<R>_n$ = 129 nm ($<R>_z$ = 133 nm) are observed from the TEM micrographs. The observation indicates that the size distribution of the spheres is rather narrow. DLS measurement results of the colloid suspension are also shown in Figure 8 (curve B). The hydrodynamic radius is independent of the scattering angle, and the size distribution is quite narrow, which is consistent with the TEM observation. Because the weight ratio of the hydrophobic to hydrophilic blocks is 94/6 for PEG_{122}-*b*-PCN_{224}, the block copolymer should easily aggregate in the solution through an irreversible phase separation process. The colloidal size is much larger than that estimated from the polymer chain length supposed of the formation of typical micelles. Because the colloids can be stably dispersed in the suspension, the aggregates could be composed of ill-defined colloidal cores and hydrophilic corona of PEG blocks attaching on the surfaces. The copolymer chains could be closely packed in the cores because of the collapse occurring in the high-water-content stage and in the process of removing THF. This point can be partially confirmed by the result that DLS and TEM give similar sizes of colloids.

The above results indicate that as the hydrophobic block length increases, the aggregates undergo a morphology transition from starlike micelles to rodlike aggregates and hollow nanotubes and finally to some colloidal spheres. A similar morphology transition has been reported for the PS-*b*-PAA and PB-PEO systems.[5−9] However, it is interesting to observe that for the hydrophobic blocks containing such strong polar side-chain groups, the block copolymers are able to self-assemble to form aggregates with well-defined morphologies. In this case, the longer PEO blocks are needed to provide the hydrophobic blocks with enough mobility to adjust their alignment during the aggregate formation process.

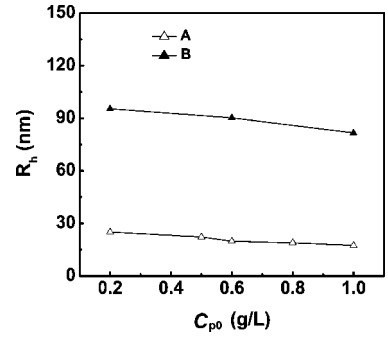

Figure 9. The relationship between the hydrodynamic radius and initial polymer concentration in THF: curve A, PEG_{122}-*b*-PCN_{24}; curve B, PEG_{122}-*b*-PCN_{224}.

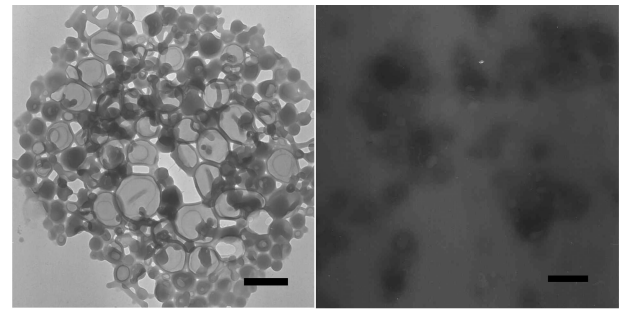

Figure 10. TEM micrographs of aggregates formed from PEG_{122}-*b*-PCN_{129} (C_{p0} = 0.5 g/L) at different water-addition rates: (A) 7.2 mL/h, scale bar = 500 nm; (B) 72 mL/h, scale bar = 200 nm.

Influence of the Preparation Conditions. It was indicated by TEM observation that in the experimental range (0.2 to 1.0 g/L), the initial polymer concentration in THF (C_{p0}) did not show an obvious influence on the aggregate morphologies of the block copolymers. Because PEG_{122}-*b*-PCN_{24} and PEG_{122}-*b*-PCN_{224} formed spherical particles, DLS was used to study the relationship between C_{p0} and $<R_h>_z$ (Figure 9). The result indicates that the average size of PEG_{122}-*b*-PCN_{24} micelles shows a slight decrease with the C_{p0} increase. Although PEG_{122}-*b*-PCN_{224} colloids show a similar tendency (Figure 9, curve B), the curve can be treated as only an apparent relationship between $<R_h>_z$ and C_{p0}. At this slow water-adding rate (0.5 mL/h), some precipitates were observed during the water-addition process and were then removed by filtration. Therefore, DLS gives only $<R_h>_z$ of the PEG_{122}-*b*-PCN_{224} colloids dispersed in the suspensions, which does not show an obvious variation with the C_{p0} change.

For the block copolymers with intermediate PEG/PCN ratios, such as PEG_{122}-*b*-PCN_{129}, the water-adding rate in the preparation process shows an obvious effect on the aggregate morphology. When the water-adding rate is low (0.5 mL/h), the block copolymers form hollow nanotubes with typical morphology given in Figure 7C. For a higher water-adding rate (7.2 mL/h), giant vesicles with coexisting colloidal spheres can be seen from TEM observation (Figure 10A). When the water-adding rate is further increased (72 mL/h), the aggregates show some less-regular low-contrast morphology (Figure 10B). As indicated by Eisenberg et al., the structure formation in the suspension can be controlled by the thermodynamic and kinetic factors.[54] When the water-adding rate is low, the aggregation of PEG_x-*b*-PCN_y more or less occurs under the thermodynamic equilibrium condition. The polymer chains can readily organize to form the ordered low-energy aggregate structures. At the intermediate water-adding rate, the structure formation is controlled by both thermodynamic and kinetic factors, which could be a more

complicated process compared with the equilibrium state. The above result seems to indicate that the nanotubes could be formed from the fusion of the giant vesicles. When the water-adding rate is too high, some intermediate and undeveloped aggregates are quenched to form the ill-defined structures.

It has been reported that the vesicular aggregates of azobenzene diblock copolymer undergo reversible dissociation and reaggregation when the suspension is alternately irradiated with UV light and visible light.[36] The variation has been attributed to a shift in the hydrophilic/hydrophobic balance induced by the light irradiation.[55] The block copolymer used in the study contains azobenzene-type chromophores with a relatively stable cis form, for which the trans/cis isomers can be switched by UV and visible light irradiation. In contrast with the azobenzene-type chromophores, the pseudostilbene-type azo chromophores of PEG_x-*b*-PCN_y possess overlapped $\pi-\pi^*$ and $n-\pi^*$ transition bands in the visible light range.[46] A strong visible light irradiation (such as Ar^+ laser irradiation) can cause very rapid trans−cis−trans isomerization cycles of the chromophores.[23,25] The possible influence of this type photoisomerization on the aggregate morphologies is still unclear and surely needs further investigation.

Conclusions

In this work, a series of amphiphilic azobenzene-containing diblock copolymers (PEG_x-*b*-PCN_y) were synthesized by ATRP and postpolymerization azo-coupling reaction. The well-defined diblock copolymers possess four different hydrophilic/hydrophobic ratios ($x = 122$, $y = 24$, 62, 129, 224) and narrow molecular weight distributions. In the aggregate formation process, the CWC is related to the polymer initial concentration in THF and the PCN block length. The CWC decreases with the increases in the PCN block length, and the dependence of CWC on the initial polymer concentration is related to the PCN block length. The morphologies of the aggregates are controlled by the PCN block length and the preparation conditions. As the PCN length increases, the block copolymers form spherical micelles, rodlike aggregates, hollow nanotubes, and colloid spheres in the suspensions. In the experimental range (0.2 to 1.0 g/L), the initial polymer concentration in THF does not show obvious influence on the aggregate morphologies of the block copolymers. For PEG_{122}-*b*-PCN_{129}, when the water-adding rate increases from 0.5 to 7.2 mL/h, the morphology of the aggregates changes from nanotubes to a mixture of giant vesicles and colloidal spheres.

Acknowledgment. Financial support from the NSFC under projects 50533040 and 20774055 is gratefully acknowledged.

Supporting Information Available: More characterization results of the block copolymers and the aggregate morphologies are given. This material is available free of charge via the Internet at http://pubs.acs.org.

References and Notes

(1) (a) Förster, S. *Top. Curr. Chem.* **2003**, *226*, 1–28. (b) Liu, S. Y.; Armes, S. P. *Curr. Opin. Colloid Interface Sci.* **2001**, *6*, 249–256. (c) Liu, T. B.; Burger, C.; Chu, B. *Prog. Polym. Sci.* **2003**, *28*, 5–26.
(2) Wilhelm, M.; Zhao, C. L.; Wang, Y. C.; Xu, R. L.; Winnik, M. A.; Mura, J. L.; Riess, G.; Croucher, M. D. *Macromolecules* **1991**, *24*, 1033–1040.
(3) Balsara, N. P.; Tirrell, M.; Lodge, T. P. *Macromolecules* **1991**, *24*, 1975–1986.
(4) Kabanov, A. V.; Nazarova, I. R.; Astafieva, I. V.; Batrakova, E. V.; Alakhov, V. Y.; Yaroslavov, A. A.; Kabanov, V. A. *Macromolecules* **1995**, *28*, 2303–2314.
(5) Zhang, L. F.; Eisenberg, A. *Science* **1995**, *268*, 1728–1731.
(6) Zhang, L. F.; Eisenberg, A. *J. Am. Chem. Soc.* **1996**, *118*, 3168–3181.
(7) Zhang, L. F.; Yu, K.; Eisenberg, A. *Science* **1996**, *272*, 1777–1779.
(8) Discher, D. E.; Eisenberg, A. *Science* **2002**, *297*, 967–973.
(9) Jain, S.; Bates, F. S. *Science* **2003**, *300*, 460–464.
(10) Noro, A.; Iinuma, M.; Suzuki, J.; Takano, A.; Matsushita, Y. *Macromolecules* **2004**, *37*, 3804–3808.
(11) Matyjaszewski, K.; Xia, J. H. *Chem. Rev.* **2001**, *101*, 2921–2990.
(12) Chiefari, J.; Chong, Y. K.; Ercole, F.; Krstina, J.; Jeffery, J.; Le, T. P. T.; Mayadunne, R. T. A.; Meijs, G. F.; Moad, C. L.; Moad, G.; Rizzardo, E.; Thang, S. H. *Macromolecules* **1998**, *31*, 5559–5562.
(13) Chong, Y. K.; Le, T. P. T.; Moad, G.; Rizzardo, E.; Thang, S. H. *Macromolecules* **1999**, *32*, 2071–2074.
(14) Bug, A. L. R.; Cates, M. E.; Safran, S. A.; Witten, T. A. *J. Chem. Phys.* **1987**, *87*, 1824–1833.
(15) Halperin, A. *Macromolecules* **1987**, *20*, 2943–2946.
(16) Zhang, L. F.; Shen, H. W.; Eisenberg, A. *Macromolecules* **1997**, *30*, 1001–1011.
(17) Shen, H. W.; Zhang, L. F.; Eisenberg, A. *J. Phys. Chem. B* **1997**, *101*, 4697–4708.
(18) Terreau, O.; Luo, L. B.; Eisenberg, A. *Langmuir* **2003**, *19*, 5601–5607.
(19) Terreau, O.; Bartels, C.; Eisenberg, A. *Langmuir* **2004**, *20*, 637–645.
(20) Gohy, J. F. *Adv. Polym. Sci.* **2005**, *190*, 65–136.
(21) Antonietti, M.; Förster, S. *Adv. Mater.* **2003**, *15*, 1323–1333.
(22) Shimizu, T.; Masuda, M.; Minamikawa, H. *Chem. Rev.* **2005**, *105*, 1401–1443.
(23) Xie, S.; Natansohn, A.; Rochon, P. *Chem. Mater.* **1993**, *5*, 403–411.
(24) Delaire, J. A.; Nakatani, K. *Chem. Rev.* **2000**, *100*, 1817–1845.
(25) Natansohn, A.; Rochon, P. *Chem. Rev.* **2002**, *102*, 4139–4175.
(26) Ikeda, T.; Horiuchi, S.; Karanjit, D.; Kurihara, S.; Tazuke, S. *Macromolecules* **1990**, *23*, 36–42.
(27) Todorov, T.; Nikolova, L.; Tomova, N. *Appl. Opt.* **1984**, *23*, 4309–4312.
(28) Rochon, P.; Batalla, E.; Natansohn, A. *Appl. Phys. Lett.* **1995**, *66*, 136–138.
(29) Kim, D. Y.; Tripathy, S. K.; Li, L.; Kumar, J. *Appl. Phys. Lett.* **1995**, *66*, 1166–1168.
(30) Finkelmann, H.; Nishikawa, E.; Pereira, G. G.; Warmer, M. *Phys. Rev. Lett.* **2001**, *87*, 015501.
(31) Li, M. H.; Keller, P.; Li, B.; Wang, X. G.; Brunet, M. *Adv. Mater.* **2003**, *15*, 569–572.
(32) Yu, Y. L.; Nakano, M.; Ikeda, T. *Nature* **2003**, *425*, 145.
(33) Li, Y. B.; He, Y. N.; Tong, X. L.; Wang, X. G. *J. Am. Chem. Soc.* **2005**, *127*, 2402–2403.
(34) Li, Y. B.; Deng, Y. H.; He, Y. N.; Tong, X. L.; Wang, X. G. *Langmuir* **2005**, *21*, 6567–6571.
(35) Tian, Y. Q.; Watanabe, K.; Kong, X. X.; Abe, J.; Iyoda, T. *Macromolecules* **2002**, *35*, 3739–3747.
(36) Wang, G.; Tong, X.; Zhao, Y. *Macromolecules* **2004**, *37*, 8911–8917.
(37) Han, Y. K.; Dufour, B.; Wu, W.; Kowalewski, T.; Matyjaszewski, K. *Macromolecules* **2004**, *37*, 9355–9365.
(38) Yang, J.; Lévy, D.; Deng, W.; Keller, P.; Li, M. H. *Chem. Commun.* **2005**, 4345–4347.
(39) Yu, H. F.; Shishido, A.; Ikeda, T.; Iyoda, T. *Macromol. Rapid Commun.* **2005**, *26*, 1594–1598.
(40) Sin, S. L.; Gan, L. H.; Hu, X.; Tam, K. C.; Gan, Y. Y. *Macromolecules* **2005**, *38*, 3943–3948.
(41) Angiolini, L.; Benelli, T.; Giorgini, L.; Salatelli, E. *Polymer* **2005**, *46*, 2424–2432.
(42) Su, W.; Luo, Y. H.; Yan, Q.; Wu, S.; Han, K.; Zhang, Q. J.; Gu, Y. Q.; Li, Y. M. *Macromol. Rapid Commun.* **2007**, *28*, 1251–1256.
(43) Yu, H. F.; Okano, K.; Shishido, A.; Ikeda, T.; Kamata, K.; Komura, M.; Iyoda, T. *Adv. Mater.* **2005**, *17*, 2184–2188.
(44) Yu, H. F.; Iyoda, T.; Ikeda, T. *J. Am. Chem. Soc.* **2006**, *128*, 11010–11011.
(45) Morikawa, Y.; Nagano, S.; Watanabe, K.; Kamata, K.; Iyoda, T.; Seki, T. *Adv. Mater.* **2006**, *18*, 883–886.
(46) Rau, H. Chapter 4. In *Photochemistry and Photophysics*; Rabek, J. F., Ed.; CRC Press: Boca Raton, FL, 1990; Vol. *II*.
(47) Wang, X. G.; Chen, J. I.; Marturunkakul, S.; Li, L.; Kumar, J.; Tripathy, S. K. *Chem. Mater.* **1997**, *9*, 45–50.
(48) Wang, X. G.; Kumar, J.; Tripathy, S. K.; Li, L.; Chen, J. I.; Marturunkakul, S. *Macromolecules* **1997**, *30*, 219–225.
(49) Wang, D. R.; Ye, G.; Wang, X. G. *Macromol. Rapid Commun.* **2007**, *28*, 2237–2243.
(50) Yabu, H.; Higuchi, T.; Shimomura, M. *Adv. Mater.* **2005**, *17*, 2062–2065.
(51) Zhang, L. F.; Eisenberg, A. *Macromolecules* **1996**, *29*, 8805–8815.
(52) Yu, Y. S.; Zhang, L. F.; Eisenberg, A. *Macromolecules* **1998**, *31*, 1144–1154.
(53) Shen, H. W.; Eisenberg, A. *Macromolecules* **2000**, *33*, 2561–2572.
(54) Yu, K.; Eisenberg, A. *Macromolecules* **1996**, *29*, 6359–6361.
(55) Tong, X.; Wang, G.; Soldera, A.; Zhao, Y. *J. Phys. Chem. B* **2005**, *109*, 20281–20287.

MA801565E